Formation and Structural Properties of Ce−Zr Mixed Oxide Nanotubes

Rodolfo O. Fuentes,*[,†] Leandro M. Acuña,[†] María G. Zimicz,[†] Diego G. Lamas,[†] J. G. Sacanell,[‡] A. Gabriela Leyva,[‡,§] and Richard T. Baker*[,||]

CINSO (Centro de Investigaciones en Sólidos), CITEFA-CONICET, J.B. de La Salle 4397, 1603 Villa Martelli, Buenos Aires, Argentina, Departamento de Física, Centro Atómico Constituyentes, CNEA, and Escuela de Ciencia y Tecnología, UNSAM, Av. Gral. Paz 1499, (1650) San Martín, Buenos Aires, Argentina, and School of Chemistry, University of St. Andrews, North Haugh, St. Andrews, Fife KY16 9ST, United Kingdom

Received June 19, 2008. Revised Manuscript Received August 15, 2008

In this work, ZrO_2−CeO_2 mixed oxide nanotubes with 50, 70, and 90 mol % CeO_2 were synthesized following a very simple, high yield procedure, and their properties were characterized by synchrotron radiation XRD and by high resolution electron microscopy. The 50, 70, and 90 mol % CeO_2 nanotubes exhibited the tetragonal phase (t′-form and t″-form, $P4_2/nmc$ space group) or the cubic phase ($Fm3m$ space group). The nanotube walls were composed of nanoparticles with an average crystallite size ranging from 4.7 to 7.6 nm. Electron microscopy observations confirmed the size of these nanoparticles by direct observation. The SEM and TEM results showed that individual nanotubes were composed of a curved sheet of these nanoparticles. By SEM analysis, the nanotubes were found to have lengths of around 1−8 μm, diameters of around 500 nm, and wall thicknesses of 20 nm. Elemental analysis showed that Ce:Zr ratios appeared to be constant across space, suggesting compositional homogeneity in the samples. The 90 mol % CeO_2 nanotubes exhibited the highest value of specific surface area, 101 $m^2 \cdot g^{-1}$, which compared with about 28 $m^2 \cdot g^{-1}$ for the other two compositions.

Introduction

ZrO_2−CeO_2 substitutional solid solutions have attracted much interest in recent years due to their extensive use in different fields, for example, as active supports or "oxygen buffers" in three-way catalysts (which are applied in controlling the emissions of NO_x, CO, and hydrocarbons from automotive exhausts). The redox behavior, thermal stability, and catalytic performance of zirconia−ceria mixed oxides are strongly related to their crystal structure. In particular, the metastable forms of the tetragonal phase have been widely investigated since they are the most suitable for technological applications.[1,2] The wide use of these systems as catalyst components has prompted a renewed interest in the preparation of these materials in the form of nanosized, high surface area powders. In this context, the present contribution describes the synthesis of Ce−Zr mixed oxide nanotubes, by a novel, simple, and high-yielding method, and the structural and chemical characterization of these materials.

Zirconia−ceria solid solutions have better catalytic properties than pure ceria. This makes these compositions of potential interest for application in catalysts for solid oxide fuel cell (SOFC) systems. Since the range of desirable operating temperatures of such systems extends from around 600 to 1000 °C, an important further advantage in this respect is the much improved thermal and chemical stability of the solid solutions over pure ceria. Evidence for the improved stability of these materials is provided by the particular case of their application in automotive catalytic converters, in which CeO_2 is present as a solid solution with ZrO_2. Without the addition of ZrO_2, CeO_2 deactivates rapidly. In contrast, CeO_2−ZrO_2 mixtures maintain their activity for many years under very harsh environments. [3]

One of the most notable characteristics of some zirconia-based solid solutions is the existence of three tetragonal forms, all belonging to the $P4_2/nmc$ space group. [4,5] The stable tetragonal form is called the t-form. There is also a t′-form with a wider solubility, but unstable in comparison with the mixture of the t-form and cubic phase. Finally, the t″-form has an axial ratio, c/a, of unity, but with the oxygen atoms displaced along the c axis from the ideal sites of the cubic phase (8c sites of the $Fm3m$ space group). In a previous study employing synchrotron radiation X-ray diffraction (SR-XRD) study,[6] we investigated the crystal structure of nanocrystalline ZrO_2−CeO_2 solid solutions. The t′/t″ and t″/cubic compositional boundaries were determined to be (68

* Corresponding authors. E-mail: rfuentes@citefa.gov.ar (R.O.F.), rtb5@st-andrews.ac.uk (R.T.B.).
† CITEFA-CONICET.
‡ CNEA.
§ UNSAM.
|| University of St. Andrews.

(1) Kaspar, J. Fornasiero, P. In *Catalysis by Ceria and Related Materials*; Trovarelli, A., Ed.; Imperial College Press: London, 2002, Ch. 6.
(2) Di Monte, R.; Kaspar, J. *J. Mater. Chem.* **2005**, *15*, 633.
(3) Gonzalez-Velasco, J. R.; Gutierrez-Ortiz, M. A.; Marc, J. L.; Botas, J. A.; Gonzalez-Marcos, M. P.; Blanchard, G. *Appl. Catal., B* **1999**, *22*, 167.
(4) Yashima, M.; Arashi, H.; Kakihana, M.; Yoshimura, M. *J. Am. Ceram. Soc.* **1994**, *77*, 1067.
(5) Yashima, M.; Sasaki, S.; Yamaguchi, Y.; Kakihana, M.; Yoshimura, M.; Mori, T. *Appl. Phys. Lett.* **1998**, *72*, 182.

10.1021/cm801680c CCC: $40.75
Published on Web 11/08/2008

± 2) and (85 ± 5) mol % CeO2, respectively. The tetragonal-to-cubic transition in these solid solutions has also been investigated by Raman and X-ray absorption spectroscopies.[7] The tetragonal/cubic phase boundary determined by SR-XRD was confirmed by Raman spectroscopy.

The preparation of nanotubes of Zr−Ce mixed oxides is attractive for several reasons. First, nanotubes with sufficiently small dimensions would have high specific surface areas (SSAs) which would lead to high activities, good atomic efficiencies and rapid response to changing conditions in catalyst systems. Second, the tubular nanostructure, in itself, may confer additional advantages, such as higher thermal, chemical and structural stability. Third, these structures may lead to completely new applications in nanotechnology, for example, if the nanotubes could be aligned.

Several routes have been used for the synthesis of compositionally homogeneous nanocrystalline ZrO_2-CeO_2 solid solutions, including the sol−gel method,[8] hydrothermal synthesis,[9] the polymerized complex method,[10] the microemulsion method,[11] the amorphous citrate process,[12] and gel combustion.[13] However, there are no reports in the literature on nanotubes of ZrO_2-CeO_2. A few studies have, however, been reported on the fabrication of CeO_2 nanotubes. Tang et al. reported the production of CeO_2 nanotubes prepared via controlled annealing from $Ce(OH)_3$ nanotubes.[14] Lu et al. reported a simple route in the synthesis of CeO_2 nanotubes within an anodic alumina membrane.[15] CeO_2 nanotubes have been synthesized with a simple solid−liquid interface reaction route in the absence of any surfactants and catalytic measurement showed that these nanotubes were very active for CO oxidation and that at 250 °C the conversion rates over CeO_2 nanotubes were three times higher than over the bulk material.[16]

Despite the fact that ZrO_2 is an interesting functional material, there are few reports on the preparation of ZrO_2 nanotubes in the literature. In 1997, Rao et al. reported on the formation of zirconia- and yttria-stabilized zirconia nanotubes prepared by first coating carbon nanotubes appropriately with the oxide material and then burning off the carbon of the template.[17] ZrO_2 nanotubes have also been synthesized by a sol−gel method using an alumina template.[18] Shin et al. reported on the synthesis of zirconia nanotubes with a precise control of wall thickness by employing atomic layer deposition and using a nanoporous polycarbonate membrane as the template.[19]

The template synthesis method for the preparation of nanomaterials, particularly by employing polymeric filtration membranes and similar materials, has been developed by Martin and co-workers,.[20,21] A recent complete review of template-directed synthesis of oxide nanotubes was presented by Bae et al. [22]

In the present work, we report, for the first time, on the preparation of CeO_2-ZrO_2 mixed oxide nanotubes using such a technique. The nanotubes were synthesized using a commercial polycarbonate membrane (with pore size of 800 nm) as a template. Three compositions were prepared with CeO_2 contents of 50, 70, and 90 mol %, and these are referred to below as ZC50, ZC70, and ZC90, respectively. The resulting nanotubes were characterized by employing synchrotron radiation X-ray diffraction (SR-XRD), scanning and high resolution transmission electron microscopy (SEM and HRTEM), and energy dispersive X-ray spectroscopy (EDS).

Experimental Procedure

Cerium nitrate hexahydrate (99.99%, Aldrich) and zirconium dinitrate oxide (99.9%, Alfa Aesar) were employed as precursors. Each nitrate was dissolved in pure H_2O separately, and then both solutions were mixed to obtain a 1 M nitrate solution with a molar Ce:Zr stoichiometry appropriate for the preparation of ZrO_2-CeO_2 mixed oxides with 50, 70, and 90 mol % CeO_2.

Templates consisting of porous polycarbonate films were used as filters in an appropriate syringe filtration system to ensure that the total volume of the pores was filled with the nitrate precursor solution. The polycarbonate (PC) films used were commercially available Isopore membrane filters from Millipore. Films with 800 nm pore pass diameters were used. The reaction to obtain the desired compound proceeded by the dehydration and denitrification of the confined precursor in a commercial microwave oven. By adjusting the time and the energy applied to the sample it was possible to accomplish this reaction without causing damage to the PC film.[23] For all compositions, an output power of 800 W was applied for a duration of 3 min. By XRD analysis, the product obtained after this process showed an amorphous structure. The desired compound was finally obtained, and the template was burnt off in a standard furnace employing a thermal treatment in which the final step involved heating in air at 650 °C for 10 min. After this treatment, the furnace was allowed to cool freely to room temperature. The resulting material was a collection of tubular nanostructures whose diameters depended on the size of the pores

(6) Lamas, D. G.; Fuentes, R. O.; Fábregas, I. O.; Fernández, M. E.; Lascalea, G. E.; Casanova, J. R.; Walsöe, N. E.; Craievich, A. F. *J. Appl. Crystallogr.* **2005**, *38*, 867.
(7) Fabregas, I. O.; Fuentes, R. O.; Lamas, D. G.; Fernandez de Rapp, M. E.; Walsoe de Reca, N. E.; Fantini, M. C. A.; Craievich, A. F.; Millen, R. P.; Temperini, M. L. A. *J. Phys.: Condens. Matter* **2006**, *18*, 7863.
(8) Rossignol, S.; Gerard, F.; Duprez, D. *J. Mater. Chem.* **1999**, *9*, 1615.
(9) Cabañas, A.; Darr, J. A.; Lester, E.; Poliakoff, M. *J. Mater. Chem.* **2001**, *11*, 561.
(10) Yashima, M.; Ohtake, K.; Kakihana, M.; Yoshimura, M. *J. Am. Ceram. Soc.* **1994**, *77*, 2773.
(11) Martinez-Arias, A.; Fernandez-Garcia, M.; Ballesteros, V.; Salamanca, L. N.; Conesa, J. C.; Otero, C.; Soria, J. *Lagmuir* **1999**, *15*, 4796.
(12) Kaspar, J.; Fornasiero, P.; Balducci, G.; Di Monte, R.; Hickey, N.; Sergo, V. *Inorg. Chim. Acta* **2003**, *349*, 217.
(13) Lamas, D. G.; Lascalea, G. E.; Juárez, R. E.; Djurado, E.; Pérez, L.; Walsöe, N. E. *J. Mater. Chem.* **2003**, *13*, 904.
(14) Tang, C.; Bando, Y.; Liu, B.; Golberg, D. *Adv. Mater.* **2005**, *17*, 3005.
(15) Kay-Lu, Y.; Guo-Ling, R.; Yu-Heng, B.; Ji-Jun, Z. *Mater. Sci. Eng. B* **2005**, *139*, 197.
(16) Guozhu, C.; Caixia, X.; Xinyu, S.; Wei, Z.; Yi, D.; Sixiu, S. *Inorg. Chem.* **2008**, *47*, 723.
(17) Rao∗, C. N. R.; Satishkumar, B. C.; Govindaraj, A. *Chem. Commun.* **1997**, 1581.
(18) Bao, J.; Xu, D.; Zhou, Q.; Xu, Z. *Chem. Mater.* **2002**, *14*, 4709.
(19) Shin, H.; Jeong, D.-K.; Lee, J.; Sung, M. M.; Kim, J. *Adv. Mater.* **2004**, *16*, 1197.
(20) Martin, C. R. *Science* **1994**, *266*, 1961.
(21) Martin, C. R. *Chem. Mater.* **1996**, *8*, 1739.
(22) Bae, C.; Yoo, H.; Kim, S.; Lee, K.; Kim, J.; Sung, M. M.; Shin, H. *Chem. Mater.* **2008**, *20*, 756.
(23) Leyva, A. G.; Stoliar, P.; Rosenbusch, M.; Lorenzo, V.; Levya, P.; Albonettib, C.; Cavallini, M.; Biscarini, F.; Troiani, H. E.; Curiale, J.; Sanchez, R. D. *J. Solid State Chem.* **2004**, *177*, 3949.

of the template used. A similar process was recently used for the synthesis of $La_{0.6}Sr_{0.4}CoO_3$ nanotubes. [24]

Synchrotron XRD experiments were carried out using the D10B-XPD beamline of the LNLS (Brazilian light facility, Campinas, Brazil) in static air. A high-intensity (low-resolution) configuration, without a crystal analyzer, was employed. The wavelength was set at 1.5496 Å. Data in the angular region of $2\theta = 18-105°$ were collected at room temperature in a step-scanning mode, with a step length of 0.05° and a step-counting time of 3 s.

SSA measurements were carried out using Brunauer, Emmett, and Teller (BET) analysis by nitrogen adsorption (ASAP 2010, Micromeritics).

SEM images were obtained using a Philips XL30 E-SEM instrument with a field emission gun. TEM images, elemental maps, and selected area electron diffraction (SAED) patterns of the nanotube sample were obtained using a JEOL 2010 TEM instrument with a LaB_6 filament and equipped with energy dispersive X-ray spectroscopy (EDS) and a Gatan digital camera. Samples were prepared by dipping a 3 mm copper grid coated with holey carbon film into a dispersion of the sample powder in hexane.

In order to determinate qualitatively the oxidation state of nanotube samples, XANES (X-ray absorption near edge structure) spectra were collected at the D04B-XAFS1 beamline at LNLS (Brazilian Synchrotron Light Laboratory) in transmission mode using a Si(110) monochromator for the Ce L_{III} edge. The energy for the Ce L_{III} edge was calibrated using Cr foil. XANES spectra at room temperature on the Ce L_{III} edge were recorded for each sample between 5710 and 5750 eV using steps of 0.2 eV. Several acquisitions (around four spectra) were carried out on the same sample to improve the signal-to-noise ratio.

Results and Discussion

Synchrotron XRD patterns recorded at room temperature for the ZC50, ZC70, and ZC90 nanotube samples (Figure 1a) exhibited resolvable peaks but with relatively severe line broadening. This broadening was ascribable to the presence of small crystallites. The average crystallite size, D_{XRD}, was determined using the Scherrer formula, [25] $D = 0.9\lambda/(\beta \cos \theta)$, where λ is the wavelength of the radiation, β is the corrected peak width at half-maximum intensity (FWHM in radians), and θ is the peak position. Since the line shape was approximately Lorentzian for all the samples, the value of β was corrected using the formula $\beta = \beta_m - \beta_{ins}$, where β_m is the measured peak width and β_{ins} is the instrumental broadening. Errors in crystallite size were derived by estimating the error in the FWHM to be equal to the 2θ step.[6]

In Table 1, results of average crystallite size, BET SSA, and the primary particle size, d_{BET}, calculated from the BET data, are summarized. The d_{BET}/D_{XRD} ratios in the ZC50 and ZC70 samples were about 6, indicating that the crystallites in both samples were agglomerated. In contrast, the ZC90 sample exhibited the highest SSA value and a low degree of agglomeration.

The 2θ region in the vicinity of the 400 and 004 reflections is inset in Figure 1a. A splitting of these peaks is expected for the tetragonal phase, indicating $c/a > 1$. However, this splitting is not evident for the ZC50 sample but a strong asymmetry is observed in this peak. In addition, by assuming the existence of two peaks here, the better fit of this profile is obtained. In contrast, only one peak is observed in the ZC70 and ZC90 samples, indicating that the cations are on the ideal fluorite sites ($c/a = 1$).

SR-XRD was carried out on the ZC50 nanotube material in order to detect the very weak 112 reflection. However, because the small crystallites (4.8 nm) gave rise to very broad

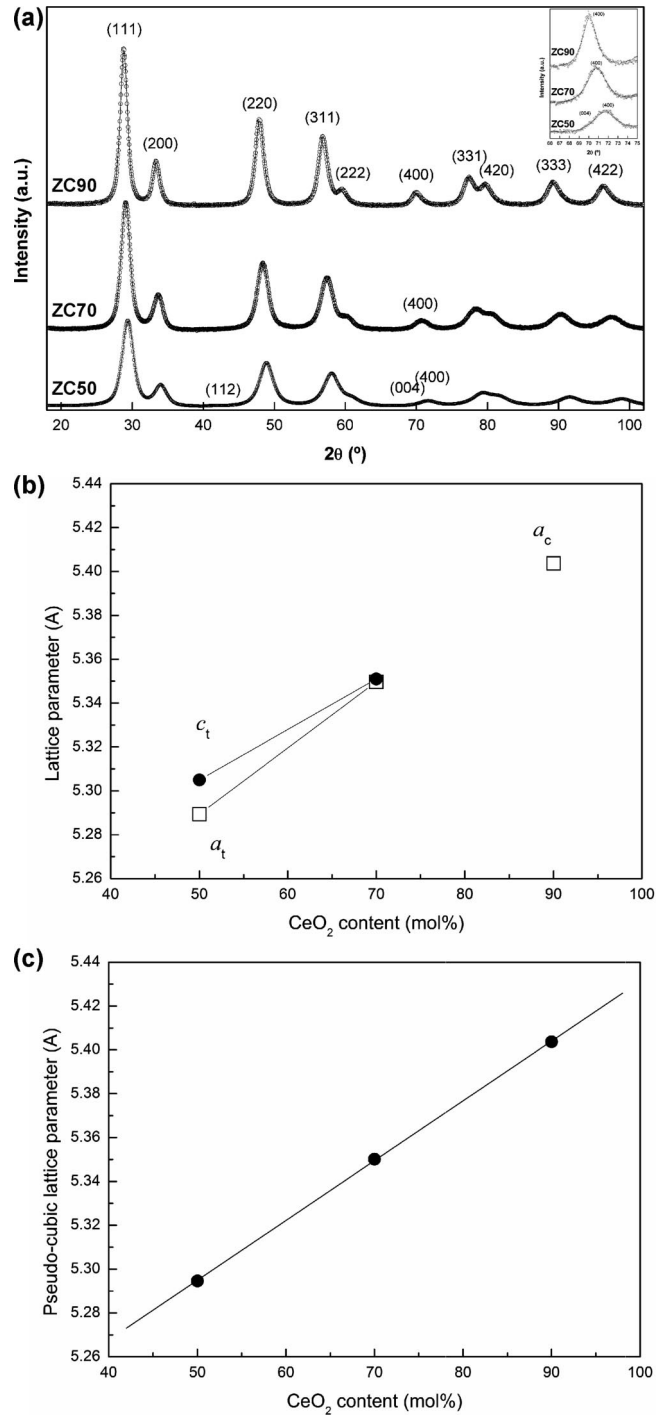

Figure 1. (a) Synchrotron XRD pattern recorded at room temperature for the three compositions of Ce−Zr mixed oxide nanotubes with inset showing the region of the 400 and 004 peaks; (b) Lattice parameters versus CeO_2 content; (c) the pseudocubic lattice parameter versus CeO_2 content. In (b) a_t and c_t correspond to the tetragonal phase, while a_c corresponds to the cubic phase. In (c), $a^* = (2a + c)/3$ and the solid line is a linear fit.

(24) Bellino, M. G.; Sacanell, J. G.; Lamas, D. G.; Leyva, A. G.; de Reca, N. E. W. *J. Am. Chem. Soc.* **2007**, *129*, 3066.
(25) Klug, H. Alexander, L. In *X-ray Diffraction Procedures for Polycrystalline and Amorphous Materials*; John Wiley: New York, 1974; p 618.

Table 1. Average Crystallite Size of Zr−Ce Mixed Oxide Nanotubes As Calculated by Scherrer's Equation and SSA

sample	formula	D_{XRD}, nm	A, $m^2\ g^{-1}$	d_{BET}, nm	d/D ratio
ZC90	$Ce_{0.9}Zr_{0.1}O_2$	7.6(1)	101.8(6)	8.2	1.1
ZC70	$Ce_{0.7}Zr_{0.3}O_2$	6(4)	24.5(9)	34.4	5.7
ZC50	$Ce_{0.5}Zr_{0.5}O_2$	4.7(2)	28.7(6)	29.9	6.4

Table 2. Structural Parameters and Standard Rietveld Agreement Factors for Zr−Ce Mixed Oxide Nanotubes[a]

sample	ZC50	ZC70		ZC90
formula	$Ce_{0.5}Zr_{0.5}O_2$	$Ce_{0.7}Zr_{0.3}O_2$		$Ce_{0.9}Zr_{0.1}O_2$
space group	$P4_2/nmc$	$P4_2/nmc$	$Fm3m$	$Fm3m$
a (Å)	5.2894(6)	5.3497(6)	5.35448(7)	5.4037(2)
c (Å)	5.305(1)	5.351 (2)		
c/a	1.0029(7)	1.0002(3)	1	1
R_p	4.29	3.75	3.09	4.85
R_{wp}	4.98	3.90	3.34	4.67
R_e	2.39	2.18	2.18	2.24

[a] For $Ce_{0.7}Zr_{0.3}O_2$, it was not possible to discriminate between the $P4_2/nmc$ and the $Fm3m$ structural models.

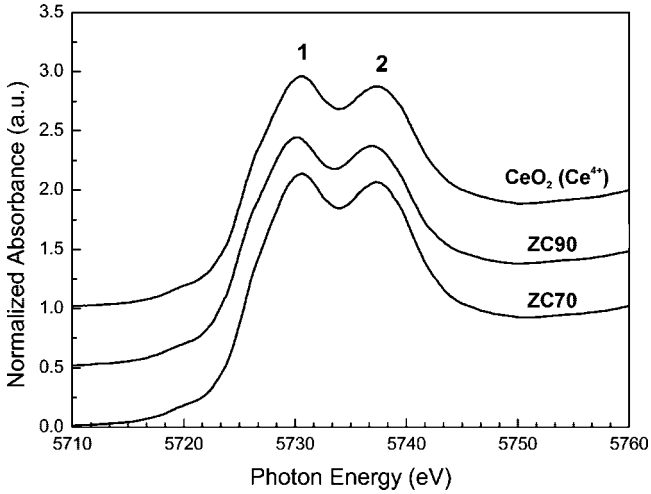

Figure 2. Ce L_{III}-edge XANES normalized absorption spectra for bulk CeO_2 and ZC70 and ZC90 nanotube samples.

Bragg reflections, the 112 peak was not observed, even though long step-counting times (20 s $step^{-1}$) were used to improve the signal-to-noise ratio.

For the ZC90 composition, with a cubic structure, the 112 reflection is forbidden, while in compositions close to the tetragonal-cubic phase boundary, that is, 70 mol % CeO_2, the detection of this peak is extremely complicated because it is rather weak and, in this particular case, suffers significant line broadening because of the small crystallite size (∼6 nm). More accurate studies for phase identification using Raman spectroscopy are planned in future work.

The structural study was performed by Rietveld refinement of the XRD data employing the program FullProf.[26] For the tetragonal phase, the $P4_2/nmc$ space group was assumed, with (Zr^{4+}, Ce^{4+}) cations and O^{2-} anions in 2a and 4d positions, respectively. For the cubic phase, the $Fm3m$ space group was assumed, with (Zr^{4+}, Ce^{4+}) cations and O^{2-} anions in 4a and 8c positions, respectively. The results of these refinements were given in terms of the usual pseudofluorite unit cell. The peak shape was assumed to be a pseudo-Voigt function. The background of each profile was fitted using a six-parameter polynomial function in $(2q)^n$, $n = 0-5$. The thermal parameters corresponding to Zr and Ce atoms were assumed to be equal.

The results of Rietveld refinements of the XRD data for the nanotube samples are summarized in Table 2. The ZC50 nanotube sample exhibited a tetragonal structure ($P4_2/nmc$ space group), specifically the t′-form, whereas the ZC90 sample exhibited a cubic structure ($Fm3m$ space group). However, for the ZC70 sample, both $P4_2/nmc$ and $Fm3m$ structural models gave similar agreement factors, and it was not possible to determine if this material exhibited an oxygen displacement.

The lattice parameters determined in this work for all three nanotube samples are reported in Table 2 and Figure 1b. These are different from those reported in our previous work on Ce−Zr mixed oxide nanopowders. [6] Figure 1c displays a plot of the pseudocubic lattice parameter, defined as $a^* = (2a + c)/3$, as a function of CeO_2 content for the nanotube samples. A remarkable linearity is apparent, indicating that compositionally homogeneous solid solutions had been formed, in concordance with $Ce_xZr_{1-x}O_2$ mixed oxide nanopowders with HSA (high surface area). [2] A significant difference is observed in the a^* values from those reported by Lamas et al. [6] These authors synthesized CeO_2-ZrO_2 nanopowders by gel-combustion with the same compositions as those studied here. These nanopowders had average crystallite sizes of about 18−20 nm. The a^* values for the nanotube materials of the present study, ZC50, ZC70, and ZC90, were found to be consistently larger than those for the nanopowders of the same composition reported by Lamas et al. In CeO_2-ZrO_2 solid solutions, a unit cell contraction is expected to occur because of the replacement of Ce^{4+} (1.01 Å) by Zr^{4+} (0.89 Å). Nevertheless, a cell expansion may also occur by reduction of Ce^{4+} to Ce^{3+}(formation of O^{2-} defects), because the ionic radius of Ce^{3+} (1.14 Å) is larger than that of Ce^{4+}. For nanocrystallites, an O^{2-} defect structure can be stabilized through surface phenomena, the importance of which decreases as the crystallite size increases.[27] It appears, therefore, that the larger a^* values in the nanotube materials can be explained by a partial reduction

(26) Rodríguez-Carvajal, J. *FullProf98*, Version 0.2; Laboratoire León Brillouin (CEA-CNRS): Saclay, France, 1998.

(27) Gennari, F. G.; Montini, T.; Fornasiero, P.; Andrade Gamboa, J. J. *Int. J. Hydrogen Energy* **2008**, *33*, 3549–3554.

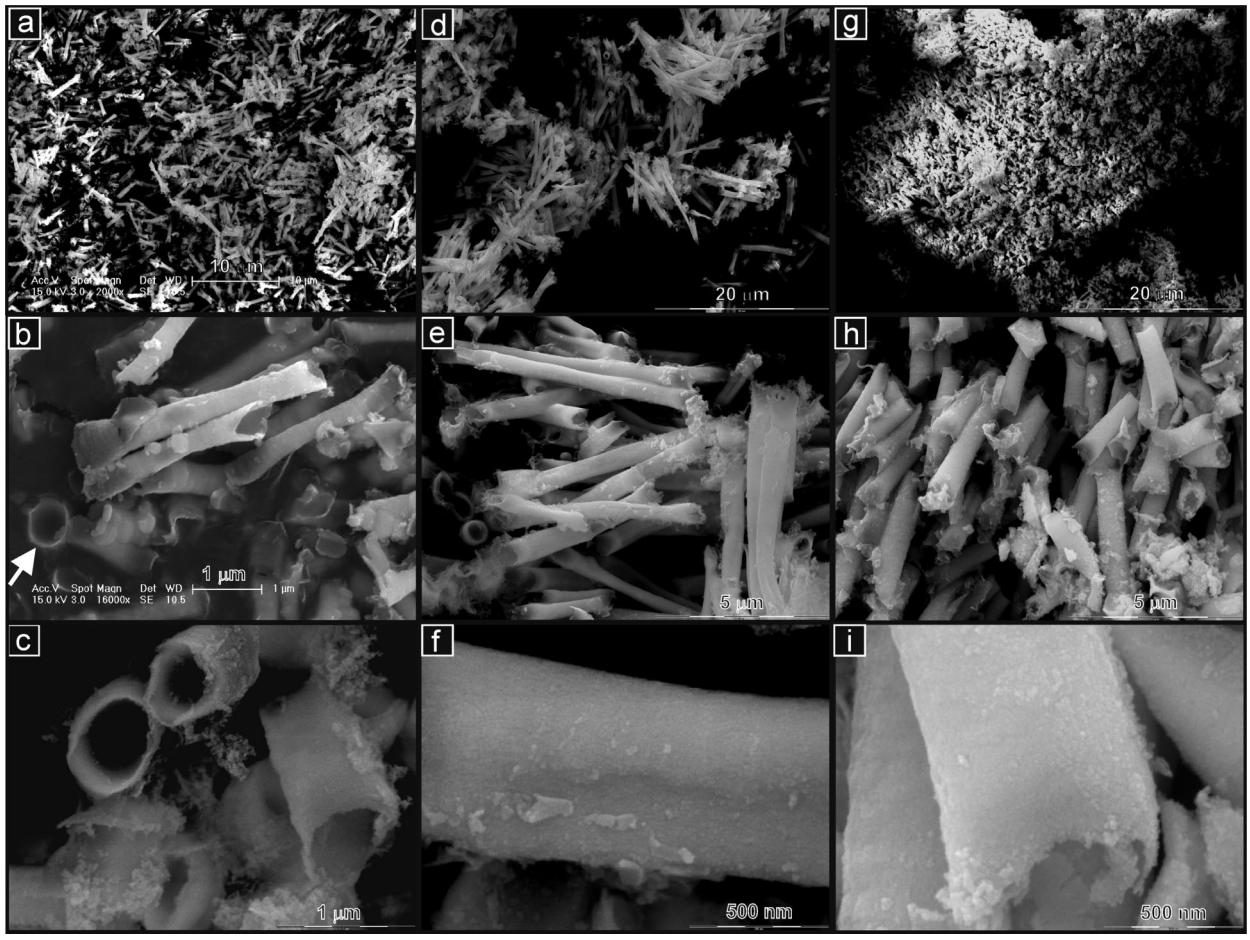

Figure 3. SEM images of (a, b) ZC50; (c−f) ZC70; and (g−i) ZC90 at low magnification, showing the high yield of nanotubes, at intermediate magnification, showing the structure of individual nanotubes, including several tubes viewed end-on; and at high magnification, showing the nanoparticulate nature of the nanotube walls.

Table 3. Mean Dimensions of Zr−Ce Mixed Oxide Nanotubes Obtained from SEM Images

sample	nanotube length, μm	σ, μm	sample size	nanotube diameter, nm	σ, nm	sample size	nanotube wall thickness, nm
ZC90	1.58	0.73	69	519	112	83	22
ZC70	3.88	1.61	117	513	106	81	19
ZC50	2.66	0.66	95	357	63	98	19

Table 4. Ce Content (at% Ce = 100 × [Ce]/{[Ce] + [Zr]}, atomic basis) from EDS and Mean Size Data of Crystallites in Zr−Ce Mixed Oxide Nanotube Walls Obtained from TEM Images

Sample	at% Ce (EDS)	d_{TEM}, nm	σ, nm	sample size	d_{VTEM}, nm
ZC90	91.3	5.9	1.7	36	6.9
ZC70	70.4	5.5	1.8	82	6.7
ZC50	52.2	5.1	1.1	26	5.6

of the Ce^{4+} to Ce^{3+}, accompanied by stabilization of the defect structure, which would be favored by the small primary particles present in the nanotube samples.

In Figure 2, the Ce L_{III} XANES spectra of the ZC70 and ZC90 nanotube samples are compared with that of the CeO_2 reference powder, in which the cerium atoms are tetravalent. Two main peaks (labeled 1 and 2) separated by approximately 7 eV are observed in the CeO_2 spectrum. These two components were also detected in the ZC70 and ZC90 samples, with an intensity ratio close to that found in the CeO_2 sample. Although the presence of Ce^{3+} ions in the nanotube samples cannot be completely excluded, based on the comparison with the reference compound, the Ce atoms appear to be mainly in the tetravalent state. The energy difference between peak 1 and peak 2 in the XANES spectra of the nanotube samples is slightly smaller than in CeO_2: about 6.5 for both the ZC70 and the ZC90 samples. This can be qualitatively explained by a shortening of the Ce−O distance. Although the Ce atom in zirconia−ceria samples is eightfold coordinated, as in CeO_2, the Ce−O mean bond length is shorter. [7]

Typical SEM micrographs of the ZC50, ZC70, and ZC90 samples are presented in Figure 3. For all three compositions, the lower magnification images clearly show the high yield of the nanotube structures. Although there is some variation between the three different compositions, the shape and size of the tubes appears to be determined to a large degree by the characteristics of the template pores. The intermediate

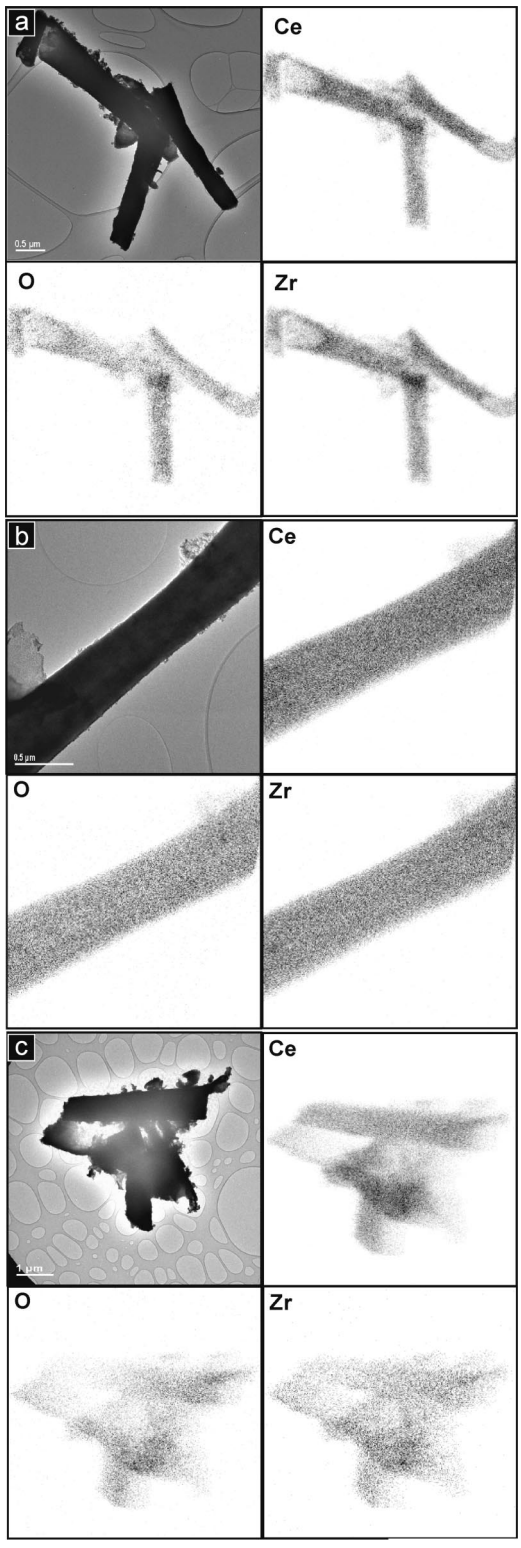

Figure 4. TEM image of groups of nanotubes with corresponding elemental maps for oxygen, zirconium, and cerium showing the correspondence between the distributions of these three elements for (a) ZC50; (b) ZC70; and (c) ZC90.

magnification SEM images show the unusual shape of the tubes, which are often narrowest at their midpoint and sometimes flared somewhat at the ends. Bands of different contrast are also seen running around the circumference of the tubes, perpendicular to their long axis. These may be caused by the layered structure of the filter template. For each composition, image analysis software was used to measure the dimensions of a large number of nanotubes from the SEM images. Histograms showing the distributions of tube length and of midtube diameter are presented in Figure S1 of the Supporting Information. Mean dimensions and other statistical data are collected together for the three compositions in Table 3. Clear variations were observed between the dimensions of the three different compositions. The largest differences are in nanotube length, which increases in the order ZC90 < ZC50 < ZC70. The ZC50 nanotubes were also narrower than those of the other two compositions, which have similar widths. The shorter, thicker tubes may result from incomplete filling of the template pores during preparation, and the smaller variation in tube diameter between the three compositions may be due to differences in behavior on calcination. During nanotube preparation, the pore volume of the template is fully filled by nitrate solution. However, when the microwave treatment is performed and the water is eliminated, it is probable that the solid material no longer completely covered the inner surface of the pores. The extent of this effect may depend on the composition of the cation nitrate solution. During the thermal treatment, two further possible effects may be involved. At low temperatures, up to approximately 260 °C (the melting point of the PC membrane), the PC membrane would expand and the diameter of the pores would therefore decrease, affecting directly the diameter of the resulting nanotube. The other important effect occurred at higher temperatures and is the sintering process. The degree of shrinkage of the material during sintering has a strong dependence on the chemical composition of the solid solution. Nevertheless, an exact explanation for the differences observed in nanotube dimensions is not possible at this stage. In a small number of images, tubes were viewed end-on (e.g., Figure 3b (arrowed) and 3c), and from these the thickness of the tube walls was measured to be around 20 nm for all three compositions. In the highest magnification images it was possible to resolve the nanocrystalline composition of the nanotube walls. For example, in Figure 3f and 3i individual crystallites of less than 10 nm can be discerned clearly.

EDS was used in the TEM to obtain X-ray emission spectra of relatively large areas (typically, one end of a nanotube) of the samples and to investigate the compositional consistency of the samples, two-dimensional elemental maps of the nanotubes. Typical EDS spectra for the three nanotube compositions are compared in Figure S2 (Supporting Information) and clearly demonstrate the increase in Ce:Zr ratio on going from ZC50 to ZC90. Values of Ce content were calculated from the EDS spectra and are presented in Table 4. These values are in good agreement with the desired elemental composition in all three materials. Elemental maps of single nanotubes or small groups of nanotubes are presented for the three different compositions in Figure 4. In each case, the TEM image can be compared directly (allowing for the slight rotation between detectors) with the elemental maps showing the distribution of oxygen, zirconium, and cerium. These elements are clearly coincident, and the intensities in the elemental maps vary in concert over space, indicating that compositional homogeneity had been

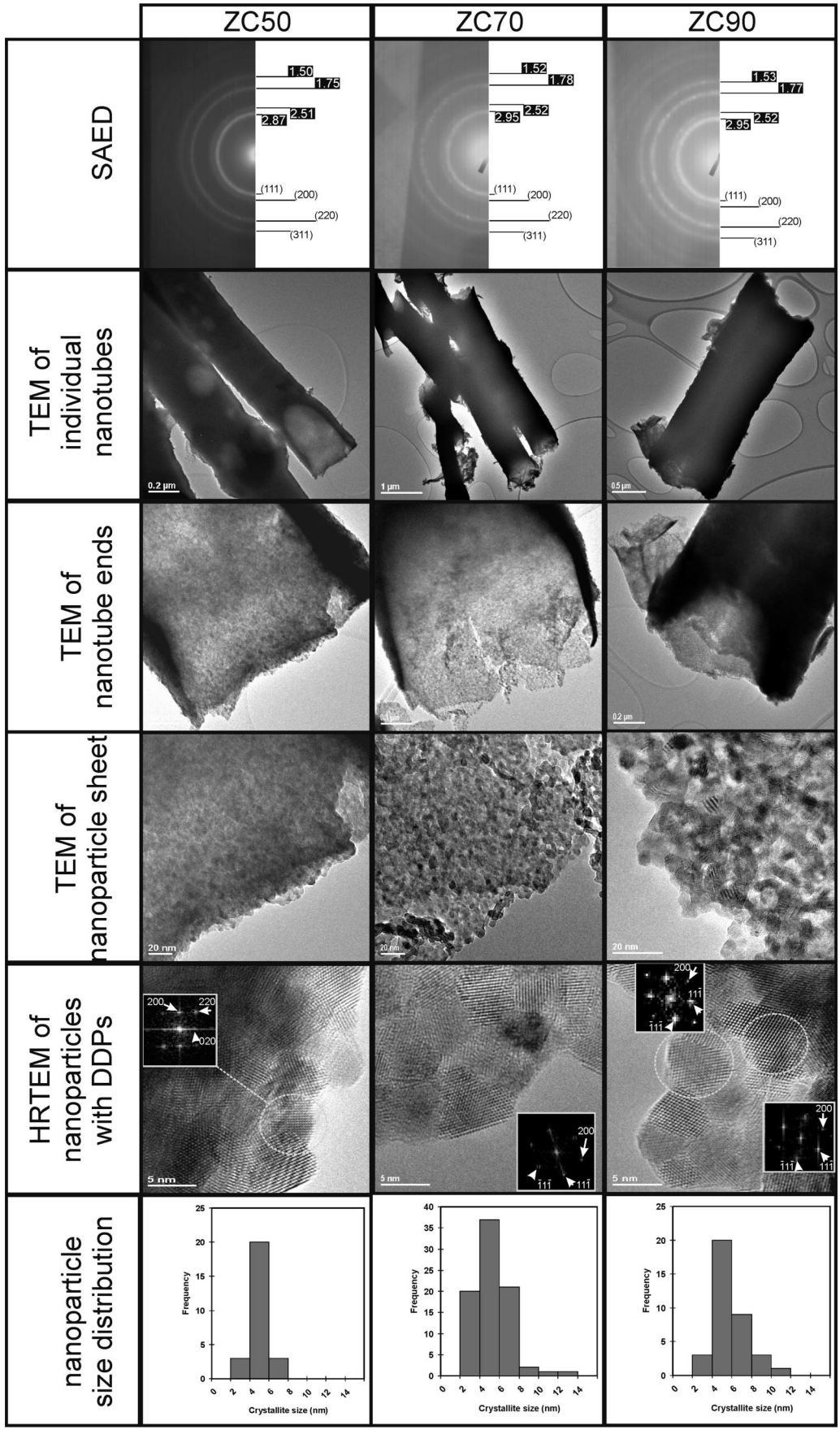

Figure 5. Comparison of SAED patterns, TEM images, and nanoparticle size distributions for the three nanotube compositions. DDPs were obtained from the HRTEM images, and these are indexed to the Fluorite structure, as indicated.

achieved in all three samples. These variations in intensity can be explained by the variation in total thickness of the sample.

Further TEM results are presented in Figure 5 for the ZC50, ZC70, and ZC90 samples. First, in the SAED patterns obtained from the end of nanotubes of the three different compositions the fact that the concentric diffraction rings are essentially continuous implies that the samples consisted of many very small crystallites. Interplanar spacings were calculated from the three patterns and can be indexed to the cubic fluorite or the tetragonal t′ phase of $Ce_xZe_{1-x}O_{2-\delta}$ in all three cases. No rings which could be assigned to the t′ phase only were visible. These would be expected to be much fainter than the rings which were observed here. This is corroborated by the SR-XRD pattern (Figure 1a) in which the (112) reflection, for example, is very weak, even for the ZC50 composition, in which it would be expected to be strongest. Second, a series of TEM images of increasing magnitude are presented for each nanotube composition. These show the shape of a single nanotube in the low magnification images and one of the ends of these nanotubes in which it can be seen that the walls are composed of a thin, curved sheet of nanoparticles, at higher magnifications. The highest magnification images clearly show several individual nanoparticles making up the edge of these sheets. Digital diffraction patterns (DDP) for selected individual crystallites are inset in these images. The DDPs can all be indexed to the fluorite phase viewed along either the [001] zone axis (for ZC50) or the [011] zone axis (for the other two compositions). Third, the width of a number of these nanoparticles was measured from each set of TEM images. The size distribution for these nanoparticles is presented in histogram form for each of the compositions in Figure 5. Mean primary crystallite sizes were calculated from these data and are presented in Table 4 as simple means (d_{TEM}) and as volume-weighted means (d_{VTEM}). These latter values can be compared directly with the values obtained from the SR-XRD data using the Scherrer equation, and they show very good agreement.

Finally, it is important to emphasize that the tubular structure of this material was maintained even after annealing treatments at 800 °C for several hours, showing only an increase in the size of the crystallites making up the nanotube walls. These findings form part of the preliminary results of an ongoing study into the effects of high temperatures and different redox conditions on these nanotube materials.[28] There is also interest in using these nanotube structures as catalyst supports for metal nanoparticles, and it is intended to investigate their catalytic activity in future work.

(28) Fuentes, R. O. Unpublished results.

Conclusions

Novel ZrO_2-CeO_2 mixed oxide nanotubes of 50, 70, and 90 mol % CeO_2 were successfully synthesized at high yield by the pore wetting method. Homogeneous elemental compositions were verified in all three samples by EDS elemental mapping of individual nanotubes. The main advantage of the polycarbonate membrane over membranes of other materials, such as alumina, is that the final compound was obtained without any traces of the template material. The structural properties of the nanotubes were studied by XRD, SR-XRD, and electron microscopy. The 50, 70, and 90 mol % CeO_2 nanotubes exhibited the tetragonal phase (t′-form and t″-form) or the cubic phase. The nanotube walls were composed of nanocrystallites, ranging from 4.7 to 7.6 nm. Particle size measurements in TEM agreed closely with the estimate obtained from the XRD data using the Scherrer equation. Nanotube dimensions were measured from the electron microscopy images. The tubes were generally of length 1−8 μm, of around 500 nm in diameter, and had wall thicknesses of about 20 nm. There was some variation in dimensions between the three different compositions, especially in length and diameter. This may have resulted from differences in behavior of the three materials during calcination. Nanotubes of 90 mol % CeO_2 exhibited the highest surface area, and for this reason this composition is a good candidate for application in catalyst systems.

The formation of O^{2-} defects (by reduction of Ce^{4+} to Ce^{3+}) seems to be responsible for the observation of larger unit cell dimensions than were found in previous work on nanopowders of the same compositions. However, the XANES results indicate that the extent of reduction of these materials is small and that the Ce^{4+} state is in the majority.

Acknowledgment. This work has been supported by the Brazilian Synchrotron Light Laboratory (LNLS, Brazil), under proposals D10B-XPD-7083 and D04B-XAFS1-7225; CONICET (Argentina, PIP No. 6559); the Agencia Nacional de Promoción Científica y Tecnológica (Argentina, PICT No. 14268 and PICT No. 38309); and the Universidad Nacional de San Martín (SA06/078). L.M.A. thanks the Fundación YPF. The TEM and SEM were performed at the Electron Microscopy Facility, University of St. Andrews, and at the CHIPS Facility, University of Dundee, respectively.

Supporting Information Available: Histograms showing size distributions of nanotube length and nanotube diameter for the three sample compositions and EDS spectra obtained in the TEM for the three compositions (PDF). This material is available free of charge via the Internet at http://pubs.acs.org.

CM801680C